Nanoscale

Accepted Manuscript

This article can be cited before page numbers have been issued, to do this please use: Y. Chu, Z. Chen, H. Zhu, L. Zhang, F. Shang, Q. Hou, L. Chen, Y. Zhang, W. Fang, Z. Cheng and Y. Zhang, *Nanoscale*, 2025, DOI: 10.1039/D4NR04586F.

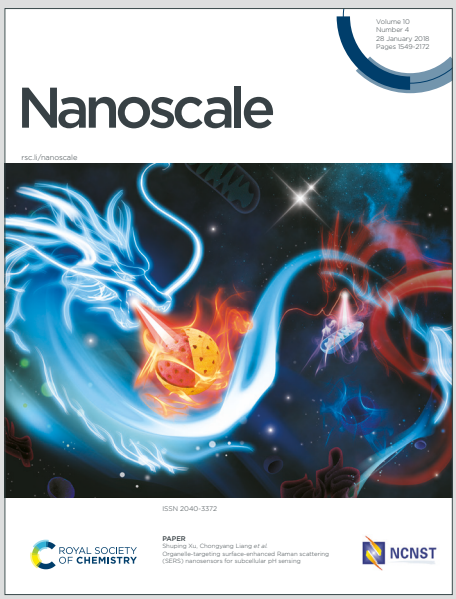

ROYAL SOCIETY OF CHEMISTRY

rsc.li/nanoscale

View Article Online
DOI: 10.1039/D4NR04586F

ARTICLE

Ultra-High Absorption Efficiency of InN Nanowires with A Wide Bandwidth in The Short-wave Infrared Range

Received 00th January 20xx,
Accepted 00th January 20xx

DOI: 10.1039/x0xx00000x

Yanmeng Chu[a], ZhouXiang Chen[a], Hanchen Zhu[a], Linjun Zhang[a], Fuxiang Shang[a], Qichao Hou[a], Lulu Chen[a], Wenzhang Fang[a,b], Yishu Zhang[a,b], Zhiyuan Cheng[a] * and Yunyan Zhang[a,b] *

The group III-V semiconductor InN is a highly promising candidate for photoelectric detectors in the short-wave infrared (SWIR) range but faces significant challenges in material quality. In recent years, the one-dimensional nanowire (NW) has allowed its high-quality growth and has added structural advantages. However, the performance potential of InN NWs is little known. Here, the optoelectrical properties of hexagonal wurtzite InN NWs are systematically studied. The high absorptivity of InN itself, along with the antenna effect and leaky model resonance, result in the InN NW exhibiting more than 99% light absorption in the 1000-1470nm range and a wide range of incidence angles (0~65°). The absorption of InN NW arrays with a low filling factor (FF) of 12.83% can be 34% higher than that of thin film materials of the same thickness, and an additional 28% enhancement can be obtained by tilting the NWs. A remarkable response up to 1 A/W can be explicitly achieved at 1550 nm with precisely arranged InN nanowire arrays. This responsivity is 11.83% higher than that of InGaAs nanowire arrays. The results indicate that InN NWs with outstanding light absorption performance can be used as an efficient photosensitive material in the SWIR range for photovoltaic, detector, and other optoelectronic devices.

Introduction

Indium nitride (InN) is a thermodynamically stable group III-V wurtzite compound that exhibits a narrow direct and nearly invariant band gap with temperature[1,2]. Currently, the bandgap of InN has been proven to be close to 0.7eV, enabling its absorption cutoff edge to precisely cover the two most crucial communication bands in the short-wave infrared (SWIR) spectrum: 1310nm and 1550nm. More importantly, the absorption coefficient of InN surpasses that of indium gallium arsenide (InGaAs) and germanium (Ge), ubiquitous materials employed in SWIR photoelectric applications. The analysis presented in Figure 1 provides a comparative evaluation of the light absorption characteristics of bulk InN against InGaAs[3] and Ge[4]. Notably, the graph illustrates that the InN exhibits a 1.8 times higher absorption coefficient than InGaAs at 1550nm. This remarkable difference underscores the profound potential of InN in advancing the fields of optics and optoelectronics in applications requiring enhanced SWIR sensitivity. In addition, InN possesses the highest electron mobility (up to 12,000$cm^2/V{\cdot}s$ at 300K[5]) within the group III-nitride semiconductors. Attribute to the advantages of nitride materials, InN can potentially achieve a high-temperature application compared with other materials. Additionally, InN demonstrates a maximum saturation velocity of $6\times10^7 cm/s$[6], and a minimum effective electron mass of $0.07m_0$[5]. These attributes, which facilitate efficient carrier transport, position InN as a highly attractive contender for a wide range of applications, including terahertz field devices[7], ultrafast optical switchers[8], high-frequency electronic devices[9], etc. Consequently, InN emerges as a promising candidate for developing next-generation optical devices.

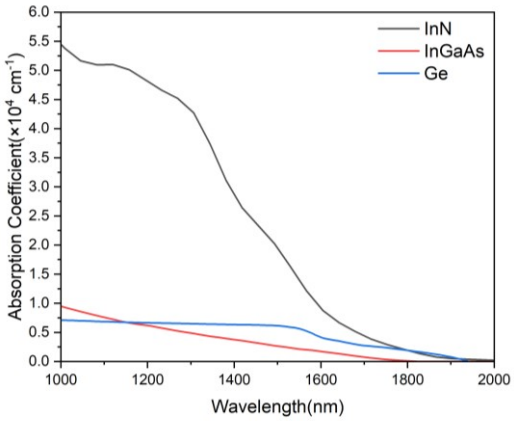

Figure 1. Comparison of the absorption coefficients of InN, InGaAs[3], Ge[4] and with the responsivity performance of detectors with the same device structure in the SWIR range.

Previously, the challenge of producing InN of superior quality arose from the difficulty in epitaxy single crystal in

[a] College of Integrated Circuits, Zhejiang University, Hangzhou, Zhejiang 311200, China. E-mail: zycheng@zju.edu.cn, yunyanzhang@zju.edu.cn.
[b] Zhejiang Technology Innovation Center of CMOS IC Manufacturing Process and Design, Hangzhou 311200, China.
Supplementary Information available: [details of any supplementary information available should be included here]. See DOI: 10.1039/x0xx00000x

appreciate substrate, resulting in a prolonged misconception regarding its band gap, which was erroneously believed to be approximately 2eV[10,11,12]. Nevertheless, the realization of higher-quality InN film grown through molecular beam epitaxy (MBE) or metal-organic chemical vapor deposition (MOCVD), along with theoretical calculations, has revealed that its actual band gap is approximately 0.7eV[13,14]. Furthermore, the exceptional characteristics of InN, including pronounced light absorption[15] and minimal inter-valley scattering[16], render it highly suitable for achieving ultra-fast response and high efficiency in the detection of SWIR wavelength ranges, particularly at the communication band of 1310/1550nm. Ultrafast and highly efficient optoelectronic conversion modules are crucial in various domains, including deep-space communication[17], last-mile access,[18] temporary link establishment, areas with vulnerable radio-frequency signal devices[19], and densely populated metropolitan areas[20].

The production of high-quality InN films is presently constrained to the process of epitaxial growth, which is mainly carried out on sapphire substrates[21] or Gallium nitride (GaN) templates[22] with 25.40% and 21.27% lattice mismatch, respectively. The epitaxy of InN films on silicon (Si) substrates directly is accompanied by a significant lattice mismatch of up to 35.24%[23], resulting in the formation of a considerable quantity of defects, thus leading to a degradation in device performance[24]. This limitation poses challenges in integrating InN devices with complementary metal-oxide-semiconductor (CMOS) technology and the scalability of the production.

One-dimensional nanowires (NWs) can alleviate the constraints through radial elastic strain relaxation, offering a cost-effective solution for high-quality integration on Si substrates.[25,26] Meanwhile, utilizing NWs as light-absorption materials for detectors also offers notable benefits. NWs have been found to exhibit enhanced light absorption per unit volume by significantly increasing light trapping compared to planar film-based devices with much less amount of material[27]. Thus, the utilization of NWs holds considerable importance in the context of small-scale detectors. Substantial investigation has been carried out on single NW[28] and periodic NW arrays[29] to find the optimum structural characteristics suitable for photodetection applications. NW arrays can support a broader range of optical absorption modes, encompassing localized[30] model, leaky model resonance, Fabry-Perot modes, and whispering-gallery modes[31], which can enhance and achieve a broad wavelength range of light absorption. In addition, a series of comprehensive electromagnetic simulations are conducted to investigate the diverse morphology-dependent absorption properties of NWs with various cross-sections, including square, circular, hexagonal, and triangular configurations[32,33]. The obtained spectra of various cross-sections exhibit qualitative similarities, such as similar absorption peaks and analogous absorption enhanced mode, but slight variations in absorption intensity. These findings indicate the excitation of similar optical resonances across all structural configurations[33]. In the case of the group III-V material, indium phosphide (InP) NW arrays with a height of 2um have demonstrated a remarkable ability to absorb over 90% of incident energy from both transverse electric (TE, where the electric field is perpendicular to the axis) and transverse magnetic (TM, where the electric field aligns parallel to the axis) polarised light, even at incidence angles of up to 60°[34,35]in the visible light band. However, the absorption properties under varying structural parameters of group III-V NW arrays and the mechanism of light absorption in the SWIR range have not been elucidated yet.

In this paper, we conduct comprehensive research on the optical absorption characteristics of single and arrays of hexagonal wurtzite InN NWs. The enhanced mode, including the antenna effect, focus effect, and leaky model resonance et al., elucidates the dependence of the absorption enhancement mechanism on NW size, height, tilt angle, and spacing over a broad wavelength spectrum. This deep understanding of their optical properties is a crucial foundation for designing next-generation, high-performance NW photoelectric detection devices.

Results and discussion

A. Absorption mode analysis

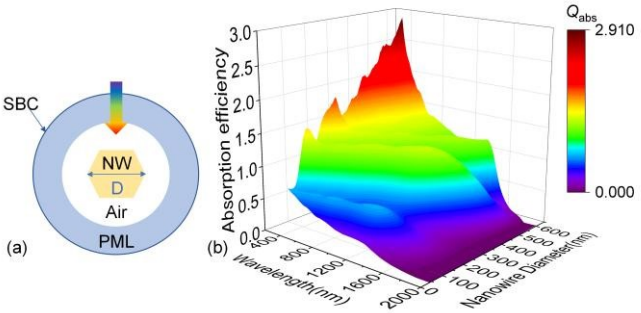

Figure 2. (a) Schematic of the 2D cross-section of single hexagonal InN NW. (b) absorption efficiency of the hexagonal InN NW as a function of wavelength(λ) and diameter(D).

All the calculational analyses were performed using the finite element method in COMSOL to reveal critical structural features determined the optical properties of hexagonal InN NWs. Figure 2(a) provides a cross-sectional illustration that schematically depicts the configuration of a single InN NW, where "D" denotes the internal dimension of the regular hexagonal NW. The single NW is surrounded by air, with a perfectly matched layer (PML) enclosing the air to capture scattered light. Additionally, a scattering boundary condition (SBC) is subject to the outer surface of the PML. It is assumed that the NW extends infinitely in the axial direction. The utilization of this reduced 2D model has proven to be a valuable method for promptly determining the absorption mode and the light absorption characteristics of NWs[32],[36]. The incident light is directed perpendicular to the NW's axis, as indicated by the rainbow arrows above the NW. This assumption is practical since light absorption primarily occurs along the axial direction. The refractive index of InN is

referenced by Wen et al.[37], while the real part of the refractive index for air set as 1, and the imaginary part as 0.

The absorption efficiency of unpolarized light is denoted as Q_{abs}, which demonstrates a significant increase of more than one across a broad spectrum of wavelengths in the case of individual NW configurations, as seen in Figure 2(b). This phenomenon means single NW possesses the capability to capture incoming photons beyond their physical cross-sectional area and thus is recognized as the "optical antenna effect"[36]. The maximum absorption is observed at shorter near-ultraviolet wavelengths, where the absorption cross-section is nearly three times its physical cross-section, suggesting that InN has a more significant potential for absorption in the ultraviolet wavelengths. The increase in diameter results in an elevated absorption within the near-ultraviolet region. Besides, as the parameter diameter increases, two distinct peaks in Q_{abs} experience a redshift, leading to plateaus that signify a notable enhancement in Q_{abs} within the SWIR region. The intensity of the higher plateau gradually rises and reaches its local maximum at D = 320nm where λ = 1245nm, with Q_{abs} reaching 132.5%, followed by a rapid decrease.

To establish the relationship between distinct enhanced absorption modes and the enhancement in the absorption of an NW, a subset of representative NW diameters that demonstrate one or more enhanced absorption peaks have been selected for further research, as indicated by grey dashed lines in Figure 3(a) and 3(b). The enhancement peaks are designated as first, second, third, etc., in ascending order of diameter. This analysis is achieved by examining the distribution of electric field intensity $|E|$ inside the NWs at the respective enhanced peaks, as illustrated in Figure 3(c)-(h). The energy flow density and direction within the NWs, i.e., the Poynting vector, are also depicted. When photons impinge upon the NW's surface, their optical trajectories experience refraction due to the high refractive index of InN compared to air, leading to a bending of optical paths. This refraction causes the incident light to converge towards the lower central region of the NW, a phenomenon referred to as the "focus effect", as illustrated by the directional energy flow arrows. Consequently, NWs exhibit an amplified nano-focusing effect and thus enhanced absorption strength. The first enhancement peak of TE arises from this focus effect, as shown in Figure 3(c).

The second peak indicates that a larger diameter NW adopts different absorption enhancement mechanisms. The absorbed incident light becomes leaky and interacts with the outside medium, carrying out a valuable antenna. Many papers have proven that leaky mode resonance (LMR)[38] can serve as the prominent contribution factor to augmentation absorption for numerous nanostructures. When the incident wavelength coincides with one of the allowed LMRs, the incident light interacts with the re-emitted light, resulting in an amplified $|E|$ intensity within the NWs. Consequently, the NW can efficiently capture and configure light inside its limits. Thus, light absorption and the subsequently generated photocurrent could be selectively heightened at a desired wavelength by adjusting the NW diameters. TE_{ml} and TM_{ml} (where "m" and "l" represent the azimuthal mode number and radial order of the resonances, respectively) correspond with distinct LMR enhancement modes as depicted in Figure 3(c)-(h). The TE_{11} mode depicted in Figure 3(d) contributes to the second highly enhanced Q_{abs} in Figure 3(a).

As the diameter of the NW continues to increase, the situation will continue to change. The third Q_{abs} peak can be ascribed to the Fabry-Perot-type modes. When light is introduced into NWs, it will be scattered or reflected by the dielectric interface; consequently, the light will constructively interfere with itself, resulting in energy stored within the resonance cavity.

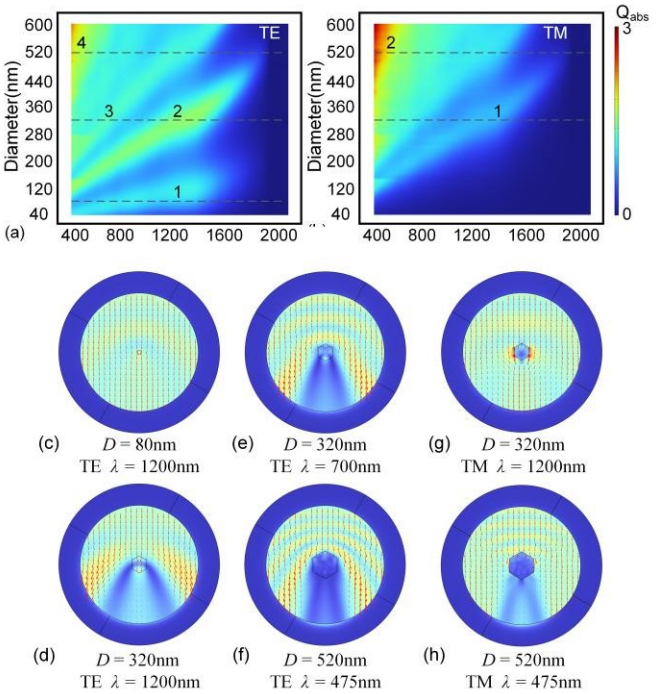

Figure 3. Q_{abs} of the single hexagonal InN NW as a function of λ and D under (a) TE and (b) TM polarized illuminations. Distribution of the electric field intensity $|E|$ inside the hexagonal InN NW for the corresponding peak indicated by grey dashed lines: (c)-(f) the 1st enhanced peak to the 4th enhanced peak under TE polarized incidence; (g)-(h) the 1st enhanced peak to the 2nd enhanced peak under TM polarized incidence.

The fourth peak combines several higher-order modes (Figure 3(f)). The hybrid mode plays a significant role in achieving the highest level of light absorption over the whole spectrum. Incident light with shorter wavelengths is prone to be absorbed at the surface, so the maximum absorption originates in the larger diameter.

Figure 3(g) demonstrates that the first enhancement in absorption associated with the TM polarized incidence arises from the resonance of the focus effect. Figure S1 depicts a distribution diagram of the magnetic field intensity $|H|$ that makes this phenomenon more apparent. The electric field intensity $|E|$ is primarily concentrated at the radial periphery of the NW, whereas it becomes negligible in the core region.

View Article Online
DOI: 10.1039/D4NR04566F

On the other hand, the field intensity associated with TM polarization is primarily localized inside the core region of the NW. This phenomenon is the reason behind the comparatively reduced absorption efficiency of TE polarization compared to TM polarization. It is notable that the second peak associated with the mixture of higher-order resonance modes, as shown in Figure 3(h), contributes considerably to the overall Q_{abs} in the short-wavelength region.

This phenomenon underscores the profound influence of NW diameter on regulating absorption modes within NWs. For photo-sensing applications such as photodetector or photovoltaic, the current density can be optimized by tuning the diameters of NWs to better match the incident wavelength to obtain the maximum response. Consequently, the Q_{abs} spectra exhibit a pronounced reliance on the individual NW parameter, matching with the distinctive resonance mode.

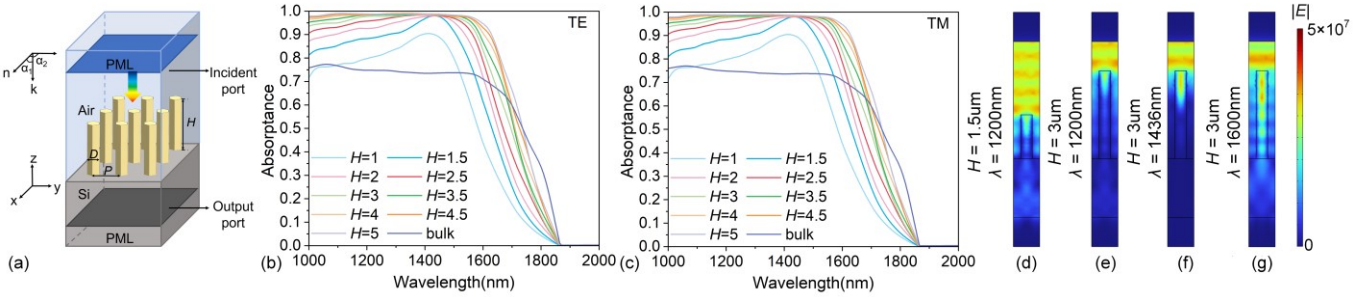

Figure 4. (a) The periodic model of the InN NW array. The absorption spectrum of NW arrays under (b) TE and (c) TM polarized incidence. (d)-(g) The longitudinal section of distribution of the electric field intensity |E| inside the 3D hexagonal InN NW under TE polarized incidence with different NW heights and incident wavelengths.

While the absorption mode of a single NW has been examined, the utilization of regularly arranged NW arrays in the device offers greater practicality for many applications such as including photodetectors[39], solar cells[40], biosensors[41], metamaterials[42], light emitters[43] and so on. The NW arrays exhibit distinct absorption characteristics compared to those of individual NW as multiple reflections of light within NW arrays are influenced by complex dimensional parameters such as height, aspect ratio between height and diameter, and spacing. It is imperative to investigate the impact of these parameters to fully exploit the potential of NW arrays.

B. Absorptance of 3D NW Array

The periodic 3D NW array model is illustrated in Figure 4(a). Assuming integration with CMOS technology, the NW arrays are grown on a Si substrate. The NW diameter is still represented as "*D*", while "*P*" signifies the period of the unit cell, and the height of the NW is represented as "*H*". Here, *D* is set to 400nm, and P is 800nm. Periodic boundary conditions are utilized to reduce computational complexity and improve processing efficiency. The periodic conditions are defined along the x and y axis, with NWs surrounded by air. The upper boundary of the air and the lower boundary of the Si substrate are designated as PMLs to capture the scattered light. The incident light is perpendicular to the x–y plane.

For the 3D NW absorption model, the absorptance A(λ) of NW arrays is given by A(λ)=1-R(λ)-T(λ), where R(λ) is the reflectance and T(λ) is transmittance. As depicted in Figure S2, the absorptance A(λ) dependence on the λ with diverse heights of Si substrate is obtained under TE polarized incidence. The Si substrate exhibits negligible absorption beyond 1000nm and essentially no absorption after 1100nm, corresponding to the Si absorption cut-off wavelength. Furthermore, it appears that the thickness of the substrate has minimal impact on the absorption characteristics of the NW arrays. In our subsequent models, the substrate thickness was set to 3um. Our primary focus lies on the absorptance of the NW arrays beyond 1000nm.

The influence of NW height on the absorptance of NW array is evaluated using absorptance obtained under TE and TM polarized incidence. The absorption spectrum exhibits similarities for both TE and TM polarized incidences, as depicted in Figure 4(b) and (c). As the NW height increases from 1 um to 3.5um, the absorptance gradually rises while the absorptance reaches the maximum at 1436nm. With continued increases in NW height, the absorptance of NW arrays reaches saturation over 95% absorptance across a wide range of wavelengths before the cut-off wavelength (~1860nm). Figure 4(b) and (c) also illustrate the absorptance of a bulk InN film with a thickness of 3um for the sake of comparison. At the same height, the NW array has a maximum absorptance increase of about 34% compared to the bulk at 1436nm, and the corresponding NW absorption is about 98%.

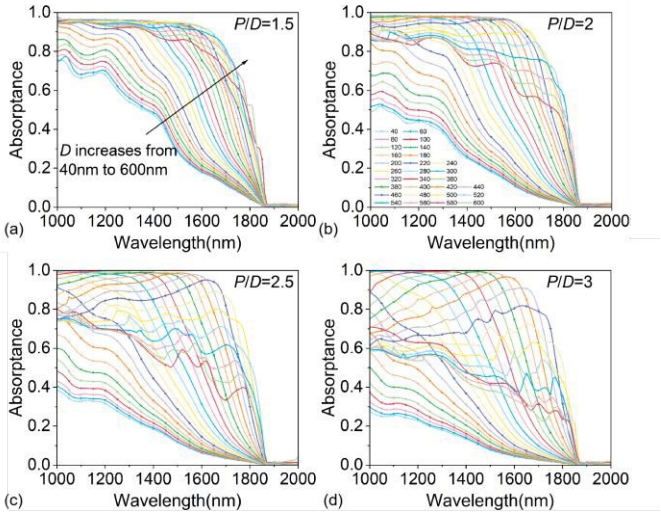

View Article Online
DOI: 10.1039/D4NR04586F

Figure 5. (a)-(d) Absorptance with the variation of P/D ranging from 1.5-3 for NW array of length H = 3um for TE polarized light.

The absorptance of bulk InN film is greater than that of InN NWs at longer wavelengths, where the transmittance of NWs considerably improves. In the spectral regions spanning from 1000 to 1500nm, it has been observed that the absorptance of a 1um-high NW array surpasses that of bulk materials with a thickness of 3um.

An examination of the normalized $|E|$ reveals that inadequate NW height results in the dispersion of residual field strength among the space between NW arrays. Consequently, for only the 1.5um height of the InN NW array, the efficient coupling of light into the NWs is hindered, as illustrated in Figure 4(d). However, when NWs reach a height of 3um, there is a higher concentration of electric field within the NWs, leading to an elevated absorptance, as shown in Figure 4(e). Enhanced absorptance is observed in Figure 4(f) when the incident light's wavelength matches the dimensions of the NW as the absorption length of light and strength within the NW is enhanced. For λ > 1600nm, several lobes of maxima and minima of $|E|$ appear periodically along the NWs. Despite the increase in strength of maxima $|E|$, the absorptance decreases significantly due to the majority of light being reflected from the top and transmitted through the Si substrate.

In addition to the factor of height, numerous researches have indicated that the spatial arrangement of NWs, specifically the ratio of periodicity to diameter (*P/D*), can exert a substantial influence on the absorption properties of NW arrays[29,35,44]. Figure 5(a)–(d) displays the absorptance spectra of NW arrays at different *P/D* ratios ranging from 1.5 to 3 under TE polarized incidence. Figure S3(a)-(d) plots the absorptance under TM polarized incidence. As the ratio of *P/D* grows, the competition among NWs diminishes, resulting in enhanced field concentration within the NWs. Therefore, as the *P/D* ratio exhibits a progressive increase, there is a corresponding increase in the maximum achievable absorptance, which approaches a value of unity. When the ratio P/D hits 2.5 and 3, the maximum absorptance can exceed 99% throughout a wide range of wavelengths from 1000nm to 1470nm, with the diameter ranging from 280 to 360 nm. For example, the NW with a diameter of 300 nm can achieve 99% absorptance in the wavelength range from 1000 nm to 1120 nm.

Additionally, for each P/D ratio, the absorptance versus *D* is also depicted. As the diameter increases, the absorptance initially rises, followed by saturation and eventually decreases rapidly. The absorptance of NW arrays with extremely small or large diameters own a narrow wavelength range capable of near-complete absorptance. Taking *P/D* = 2.5 as an example, when the diameter of the NW is small (<260nm), the enhancement of absorptance is mainly due to the enhanced resonance caused by the increase in diameter. As the diameter gets large, the absorptance peak caused by LMR exhibits a continuous redshift. The abrupt decline in absorption observed in the NW array can be attributed to the enhanced transmission at longer wavelengths and increased reflection off the top, both of which are consequences of the greater diameter (>460nm) of the array.

To be specific, the P/D ratio determines the overall absorptance, whereas the diameter *D* dominates the peak and mostly influences the wavelength at which peak absorptance occurs. Thus, to achieve optimal absorptance, it is imperative to meticulously tune the size of NW and the arrangement of their arrays.

In contrast to cylindrical NWs, hexagonal NWs exhibit a distinct six-fold symmetry, which leads to variations in light absorption characters at different incident angles. The absorptance at various elevation angles α_1 was initially computed, as α_1 is determined by the angle formed between the outward unit normal vector to the boundary n and the incoming wave vector *k*, as depicted in Figure 4(a). The angle of 0° denotes a scenario where light is incident vertically, whereas an angle of 90° signifies light incident in the x-direction at the uppermost part of the air layer. When the incidence elevation angle is below 40°, it is observed that the absorptance can surpass 95% across a broad range of wavelengths, while α_1 between 40° to 65°, the absorptance is as high as 90%, as seen in Figure 6(a). As α_1 increases, there is a corresponding redshift observed in the absorption peak at the longer wavelength. When the α_1 exceeds 75°, the absorptance decreases rapidly. The optical power loss spectrum and the Poynting vector of different angles α_1 at 1400nm are shown in Figure 6(c)-(e).

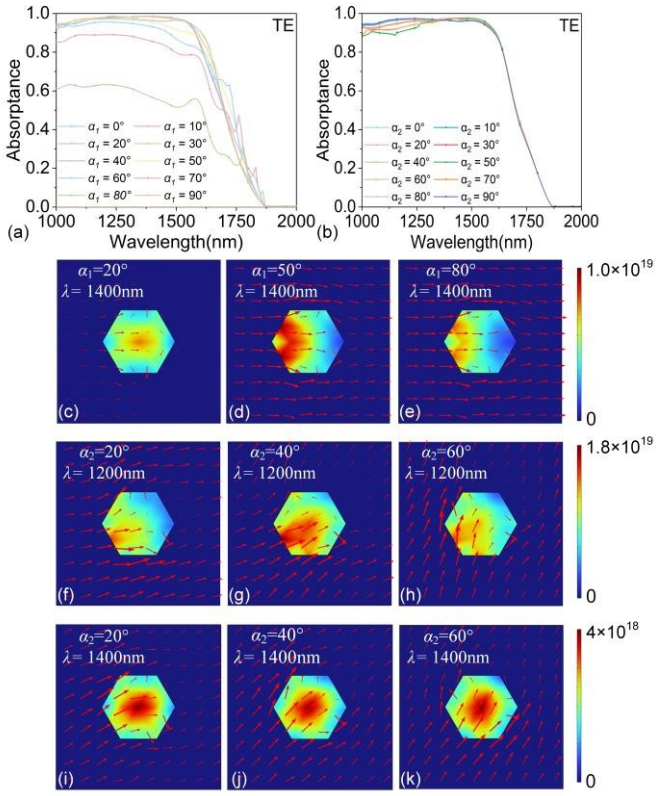

Figure 6. (a) The absorptance as a function of wavelength and elevation angle α_1. (b) The absorptance as a function of wavelength and azimuth angle α_2 when α_1 set to 40° . (c)-(e) The optical power loss spectrum and the Poynting vector of different angles α_1 at

View Article Online
DOI: 10.1039/D4NR04580F

1400nm. (f)-(k) The optical power loss spectrum and the Poynting vector of different angles α_2 at 1200nm and 1400nm.

Subsequently, theoretical calculations were to determine the impact of varying azimuth angles α_2 on the absorptance of NW arrays, assuming a fixed incident elevation angle α_1 of 40°. α_2 denotes the angle formed between the incident light and the axis while rotating within the x-y plane. An angle of 0° indicates a line parallel to the x-axis, whereas an angle of 90° degrees indicates a line parallel to the y-axis. Considering the symmetry of the hexagon, the analysis exclusively encompassed azimuth angles within the range of 0° to 90°. The results are shown in Figure 6(b). Almost all incident azimuths exhibit an absorptance of over 90% throughout the entire spectral range of concern. Due to the symmetry of the regular hexahedron, the absorptance also exhibits symmetry about 45°, with the 0° absorptance curve similar to that of 90°, and the 10° absorption curve resembling that of 80° and so on. In the spectral range below 1350nm, the absorptance exhibits the lowest efficiency when the α_2 is 45°. This can be mainly attributed to the high reflectance of the incident light at 45° and the subsequent emission of NWs. These processes contribute to an overall rise in the total reflectivity of the NW array. Figure 6(f)-(h) depicts the optical power loss spectrum and Poynting vector of the x-y plane situated at the uppermost region of the NW, specifically at α_2 equal to 20°, 40°, and 60° at wavelength 1200nm. The optimal absorptance is attained when α_2 is set at 45° beyond the wavelength of 1350nm. As seen in Figure 6(i)-(k), the absorptance predominantly occurs at the core position, primarily attributed to the enhanced penetration of long wavelength light within the NW. Currently, the incidence azimuth angle α_2 of 45° experiences a reduced impact from refraction, resulting in a higher absorption of photons.

C. Inclined InN NW array

Further, the optical pathway can be extended by enhancing the reflection among the NWs arrays, hence boosting the absorption, expanding methods to enhance absorption, and adjusting their dimensions and distributions to achieve higher absorption intensity. When NWs are aligned axially in parallel with the direction of light incidence and perpendicular to the substrate, a substantial proportion of the incident light is reflected toward the air, while just a fraction of the photons that undergo refraction and reflection along the sidewalls of NWs on the possibilities to be secondarily absorbed. One practical approach to expanding the optical pathway is accomplished by tilting the NWs at an angle relative to the substrate. Etching has been reported as an optional method to fabricate inclined Si NWs[45], while previous theoretical studies have also demonstrated that the inclined Si and GaAs NWs demonstrate enhanced absorption compared to perpendicular NWs[46,47].

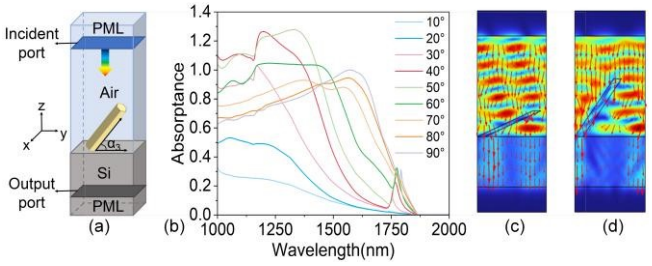

Figure 7. (a) The periodic model of inclined InN NW array. (b) The absorption spectrum of the NW array is dependent on the inclination angle α_3 under TE polarized light. The cross-section of distribution of the electric field intensity |E| inside the inclined InN NW under TE polarized incidence at λ=1300 nm:(c) α_3 = 20°, (d) α_3 = 50°.

Figure 7(a) illustrates the schematic diagram of periodic inclined NWs, characterized by a diameter of 400nm and a length of 3μm. The inclination angle α_3, denoted as the angle between the NW and the substrate, is defined as 90° signifies a perpendicular orientation to the substrate, while 0° indicates the NW lying entirely flat. The resulting absorptions of InN NWs depend on the different α_3 displayed in Figure 7(b). The absorption in the theoretical simulation falls significantly below 100%, ascribed from their *P/D* ratio being considerably lower than the ideal value of 2.5. To intuitively illustrate how inclined NWs can affect absorption, the maximal absorption of the vertical NW arrays in SWIR is normalized for all other inclined NWs. The absorption effect of tilted NWs can increase the absorption rate by a further 28%.

The NWs that possess minor α_3 from 10° to 20° show much lower absorptions than that of vertical NWs, as the diameters of these near-lying flat NWs determine the absorbed length of the incident light, which is insufficient to absorb the light. Compared to shorter wavelengths, the distribution of electric field intensity $|E|$ is predominantly localized near the border at longer wavelengths, as depicted in Figure 7(c). Hence, the absorptance in longer wavelengths is comparatively lower than in the shorter wavelengths, consistent with Figure 3(a). The absorption characteristics of NWs with an α_3 ranging from 30° to 50° exhibit enhanced absorptions compared to vertical ones. The absorption intensities exhibit a progressive augmentation and red-shift with the elevation of the α_3. The observed phenomenon can be explained by the guided-mode-fiber function of these inclined NWs, in which incident light simultaneously absorbs and undergoes multiple reflections within NWs' sidewalls. At an α_3 of 50°, the number of photons that are reflected and subsequently increases due to the propagation of reflected light along the axis of NW. Thus, the maximum absorption is obtained at the wavelength of about 1330nm, as depicted in Figure 7(d). As the α_3 is further increased, the projection area of the NWs on the substrate diminishes, leading to a reduction in the number of acceptable incident photons. Consequently, the absorption within the SWIR wavelength range experiences a decline. However, NWs with an inclination angle α_3 ranging from 30° to 70° exhibit a distinct peak around 1560 nm, which can be attributed to the resonance effect between the inclined NWs and the refraction and reflection of the incident light. The cross-sectional distribution of the electric field intensity |E| inside an inclined InN nanowire with α_3 = 50° is taken as an example, as shown in Figure S4. Thus, it has been established that manipulating the inclined angle of the NWs while simultaneously ensuring the suitable dimensions and arrangement of the NW arrays can effectively modulate the absorption.

D. Compared with InGaAs NW

Having optimized the NWs based on their optical absorption performance, further simulations of their photoelectric

properties were conducted utilizing the refined periodic structure seamlessly integrated onto a silicon substrate. The doping configuration of the repeat InN NW unit, as depicted in Figure 8(a), incorporates a P-type ohmic contact at the apical end and an N-type ohmic contact at the base interface with Si, resulting in the formation of an efficient PIN structure within the NWs. The incident light direction is perpendicular to the substrate and parallel to the NW direction, with power set to 1mW.

The responsivity curve of the InN NW array within the SWIR range is presented in Figure 8(b), achieving a remarkable responsivity of ~1 A/W at the 1550nm wavelength and the maximum responsivity can reach up to 1.16A/W at 1730 nm. This finding underscores the potential of InN NW arrays as highly effective photodetectors.

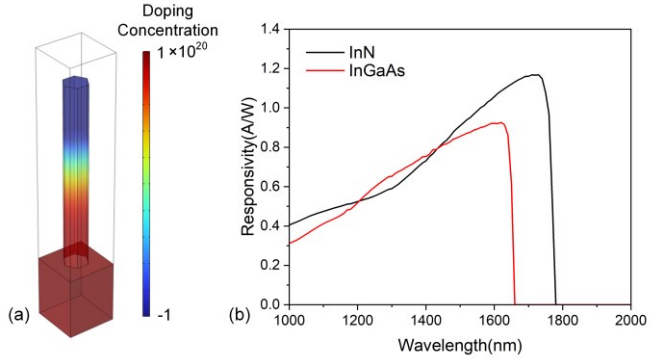

Figure 8. (a) The doping configuration of the repeat NW unit in periodic arrays. Red represents n-type doping, and blue represents p-type doping. (b) The responsivity curve of the InN and InGaAs NW array within the SWIR range.

Table 1 Optical absorptance performance of InGaAs and InN NW arrays at 155nm

	InN	InGaAs
Absorption coefficient(cm^{-1})	1.40×10^4	0.19×10^4
Light absorption efficiency	99.82%	90.18%
Responsivity(A/W)	0.99	0.89

For a comprehensive comparison, the responsivity data of InGaAs NW array with identical nanostructure and doping configurations was also included, which is also presented in Figure 8(b). Notably, the InGaAs NWs exhibit a lower responsivity of 0.89A/W at 1550nm with a maximum responsivity of 0.93A/W, further validating the superior performance of the InN NW arrays. Table 1 presents the optical absorptance performance of InGaAs and InN NW arrays at 1550nm with the same size.

Conclusions

In summary, we have proven the III-V NW arrays made of InN semiconductors are highly promising photosensitive materials in the SWIR due to their outstanding light absorption properties. Our calculation shows that the subwavelength dimensions, high refractive index and high absorption coefficient of InN NWs enable them to absorb light beyond their projected area and sustain multiple enhancement light absorption modes, resulting in approximately 99% light absorption ability performance in the wide 1000-1470nm range and incidence angles (0~65°). By adjusting the size, height, arrangement, and tilt angle of the NW arrays, even with a relatively low filling ratio and height, it is possible to achieve light absorption 28% higher than that of bulk devices with the same height. By adopting precisely optimized NW arrays, a response rate as high as 1 A/W can be achieved at the 1550nm wavelength by InN, which is 11.83% higher than that of InGaAs. Meanwhile, the maximum optical response in the SWIR range is 24.73% higher than InGaAs NW arrays. Our newly gained understanding of absorption features in individual NWs and NW arrays can now guide the rational design of high-efficiency NW-based photodetector or photovoltage cells that can operate at high temperature.

Conflicts of interest

There are no conflicts to declare.

Acknowledgments

This work was supported by the National Natural Science Foundation of China (62474163), Zhejiang Provincial Natural Science Foundation of China (Z24F040009), Zhejiang University Education Foundation Qizhen Scholar Foundation (K20240015), CMOS Special Program of Zhejiang University (04010000-K2A033208).

References

[1] Grzegory, I., Jun, J., Krukowski, S., Perlin, P. & Porowski, S. InN Thermodynamics and Crystal Growth at High Pressure of N_2. Jpn. J. Appl. Phys. 32, 343 (1993).
[2] Kumar, V. & Roy, D. R. Structure, bonding, stability, electronic, thermodynamic and thermoelectric properties of six different phases of indium nitride. J. Mater. Sci. 53, 8302–8313 (2018).
[3] Adachi, S. Optical dispersion relations for GaP, GaAs, GaSb, InP, InAs, InSb, Al x Ga1− x As, and In1− x Ga x As y P1− y. J. Appl. Phys. 66, 6030–6040 (1989).
[4] Nunley, T. N. et al. Optical constants of germanium and thermally grown germanium dioxide from 0.5 to 6.6eV via a multisample ellipsometry investigation. J. Vac. Sci. Technol. B, Nanotechnol. Microelectron. Mater. Process. Meas. Phenom. 34, (2016).
[5] Zhao, S. & Mi, Z. InN Nanowires : Epitaxial Growth, Characterization, and Device Applications. in 267 – 304 (2017).
[6] O'Leary, S. K., Foutz, B. E., Shur, M. S. & Eastman, L. F. Steady-state and transient electron transport within bulk wurtzite indium nitride: An updated semiclassical three-valley Monte Carlo simulation analysis. Appl. Phys. Lett. 87, (2005).
[7] Ascázubi, R., Wilke, I., Denniston, K., Lu, H. & Schaff, W. J. Terahertz emission by InN. Appl. Phys. Lett. 84, 4810–4812 (2004).
[8] Jia, J., Yagi, T. & Makimoto, T. Ultrafast dynamics of electronic structure in InN thin film. (2021).
[9] Ghosh, K. & Singisetti, U. Design and Analysis of High Frequency

View Article Online
DOI: 10.1039/D4NR04586F

InN Tunnel Transistors. (2013).
[10] Gucmann, F. et al. InN crystal habit, structural, electrical, and optical properties affected by sapphire substrate nitridation in N-polar InN/InAlN heterostructures. Semicond. Sci. Technol. 36, 075025 (2021).
[11] Butcher, K. S. A. & Tansley, T. L. InN, latest development and a review of the band-gap controversy. Superlattices Microstruct. 38, 1–37 (2005).
[12] Motlan, Goldys, E. M. & Tansley, T. L. Optical and electrical properties of InN grown by radio-frequency reactive sputtering. J. Cryst. Growth 241, 165–170 (2002).
[13] Wu, J. et al. Unusual properties of the fundamental band gap of InN. Appl. Phys. Lett. 80, 3967–3969 (2002).
[14] Nanishi, Y., Saito, Y. & Yamaguchi, T. RF-Molecular Beam Epitaxy Growth and Properties of InN and Related Alloys. Jpn. J. Appl. Phys. 42, 2549–2559 (2003).
[15] Andreev, B. A. et al. Towards the indium nitride laser: obtaining infrared stimulated emission from planar monocrystalline InN structures. Sci. Rep. 8, 9454 (2018).
[16] Jang, D.-J. et al. Carrier dynamics and intervalley scattering in InN. Opt. Mater. (Amst). 31, 1857–1859 (2009).
[17] Wang, Y., Guan, N., Yu, J. & Li, H. Research on Transmission Rate of Deep Space Optical Communications Based on PPM Technology. in 2022 2nd International Conference on Consumer Electronics and Computer Engineering (ICCECE) 356–359 (IEEE, 2022).
[18] Farooq, E., Sahu, A. & Gupta, S. K. Survey on FSO Communication System—Limitations and Enhancement Techniques. in 255–264 (2018).
[19] Esman, R. D., Biernacki, P. D., Nichols, L. T. & Matthews, P. J. Optoelectronics for radio frequency conversion. in Conference Proceedings. LEOS'98. 11th Annual Meeting. IEEE Lasers and Electro-Optics Society 1998 Annual Meeting (Cat. No.98CH36243) vol. 2 253–254 (IEEE).
[20] Glentis, G.-O. et al. Cost-effective adaptive optical network technologies for Metropolitan Area Networks. in 2014 16th International Conference on Transparent Optical Networks (ICTON) 1–4 (IEEE, 2014).
[21] Feng, Z. C. et al. Optical, surface, and structural studies of InN thin films grown on sapphire by molecular beam epitaxy. J. Vac. Sci. Technol. A 41, (2023).
[22] Chen, W.-C. et al. Study of InN epitaxial films and nanorods grown on GaN template by RF-MOMBE. Nanoscale Res. Lett. 7, 468 (2012).
[23] Wang, W. & Zhao, G. Lattice vibrations and optical properties of wurtzite InN in the reststrahlen region. Phys. B Condens. Matter 407, 4313–4317 (2012).
[24] Gao, F. et al. Growth of InN Nanowires with Uniform Diameter on Si(111) Substrates: Competition Between Migration and Desorption of In Atoms. Small 13, (2017).
[25] Honsberg, C., Barnett, A. & Kirkpatrick, D. Nanostructured Solar Cells for High Efficiency Photovoltaics. in 2006 IEEE 4th World Conference on Photovoltaic Energy Conference 2565–2568 (IEEE, 2006).
[26] LaPierre, R. R. Numerical model of current-voltage characteristics and efficiency of GaAs nanowire solar cells. J. Appl. Phys. 109, (2011).
[27] Wen, L. et al. Theoretical analysis and modeling of light trapping in high efficicency GaAs nanowire array solar cells. Appl. Phys. Lett. 99, (2011).
[28] Garnett, E. & Yang, P. Light Trapping in Silicon Nanowire Solar Cells. Nano Lett. 10, 1082–1087 (2010).
[29] Guan, Y., Cao, G. & Li, X. Single-nanowire silicon photodetectors with core-shell radial Schottky junction for self-powering application. Appl. Phys. Lett. 118, (2021).
[30] Hu, L. & Chen, G. Analysis of Optical Absorption in Silicon Nanowire Arrays for Photovoltaic Applications. Nano Lett. 7, 3249–3252 (2007).
[31] Liu, L. et al. Absorption and photoemission of optically localized GaN nanowire array cathode. MRS Commun. 13, 162–168 (2023).
[32] Berdnikov, Y. et al. Mapping of Fabry–Perot and whispering gallery modes in GaN microwires by nonlinear imaging. Nanotechnology 32, 40LT01 (2021).
[33] Cao, L. et al. Semiconductor Nanowire Optical Antenna Solar Absorbers. Nano Lett. 10, 439–445 (2010).
[34] Kempa, T. J. et al. Coaxial multishell nanowires with high-quality electronic interfaces and tunable optical cavities for ultrathin photovoltaics. Proc. Natl. Acad. Sci. 109, 1407–1412 (2012).
[35] Aghaeipour, M. & Pettersson, H. Enhanced broadband absorption in nanowire arrays with integrated Bragg reflectors. Nanophotonics 7, 819–825 (2018).
[36] Anttu, N. & Xu, H. Q. Coupling of Light into Nanowire Arrays and Subsequent Absorption. J. Nanosci. Nanotechnol. 10, 7183–7187 (2010).
[37] Cao, L. et al. Engineering light absorption in semiconductor nanowire devices. Nat. Mater. 8, 643–647 (2009).
[38] Mokkapati, S. & Jagadish, C. Review on photonic properties of nanowires for photovoltaics [Invited]. Opt. Express 24, 17345 (2016).
[39] Li, Z. et al. Review on III–V Semiconductor Nanowire Array Infrared Photodetectors. Adv. Mater. Technol. 8, (2023).
[40] Mukherjee, A. et al. GaAs/AlGaAs Nanowire Array Solar Cell Grown on Si with Ultrahigh Power-per-Weight Ratio. ACS Photonics 8, 2355–2366 (2021).
[41] Li, D. et al. A supersensitive silicon nanowire array biosensor for quantitating tumor marker ctDNA. Biosens. Bioelectron. 181, 113147 (2021).
[42] Tekcan, B. et al. Semiconductor nanowire metamaterial for broadband near-unity absorption. Sci. Rep. 12, 9663 (2022).
[43] Yulianto, N. et al. Wafer-scale transfer route for top–down III-nitride nanowire LED arrays based on the femtosecond laser lift-off technique. Microsystems Nanoeng. 7, 32 (2021).
[44] Azizur-Rahman, K. M. & LaPierre, R. R. Wavelength-selective absorptance in GaAs, InP and InAs nanowire arrays. Nanotechnology 26, 295202 (2015).
[45] Meng, X. et al. Stable Superwetting Surface Prepared with Tilted Silicon Nanowires. Nano-Micro Lett. 8, 388–393 (2016).
[46] Kordrostami, Z. & Sheikholeslami, H. Optimization of light trapping in square and hexagonal grid inclined silicon nanowire solar cells. Opt. Commun. 459, 124980 (2020).
[47] Zamani, M., Kordrostami, Z. & Hamedi, S. Efficient inclined core-shell nanowire solar cells. Optik (Stuttg). 248, 167974 (2021).

View Article Online
DOI: 10.1039/D4NR04586F

Data Availability Statement

The authors confirm that the data supporting the findings of this study are available within the article and its supplementary materials.